LAWRENCE
LIVERMORE
NATIONAL
LABORATORY

LLNL-JRNL-417021

Quantifying Transient States in Materials with the Dynamic Transmission Electron Microscope

G. Campbell, T. LaGrange, J. Kim, B. Reed, N. Browning

September 22, 2009

Journal of Electron Microscopy - Oxford

Disclaimer

This document was prepared as an account of work sponsored by an agency of the United States government. Neither the United States government nor Lawrence Livermore National Security, LLC, nor any of their employees makes any warranty, expressed or implied, or assumes any legal liability or responsibility for the accuracy, completeness, or usefulness of any information, apparatus, product, or process disclosed, or represents that its use would not infringe privately owned rights. Reference herein to any specific commercial product, process, or service by trade name, trademark, manufacturer, or otherwise does not necessarily constitute or imply its endorsement, recommendation, or favoring by the United States government or Lawrence Livermore National Security, LLC. The views and opinions of authors expressed herein do not necessarily state or reflect those of the United States government or Lawrence Livermore National Security, LLC, and shall not be used for advertising or product endorsement purposes.

Quantifying Transient States in Materials with the Dynamic Transmission Electron Microscope

Geoffrey H. Campbell,[1] Thomas LaGrange,[1] Judy S. Kim,[2] Bryan W. Reed,[1] Nigel D. Browning[1,3]

[1] Condensed Matter and Materials Division, Physical and Life Sciences Directorate, Lawrence Livermore National Laboratory, PO Box 808, Livermore, CA 94550 USA

[2] Department of Materials, University of Oxford, Parks Rd., Oxford, OX1 3PH, UK

[3] Department of Chemical Engineering and Materials Science and Department of Molecular and Cellular Biology, University of California–Davis, One Shields Ave., Davis, CA 95616 USA

Keywords: In situ microscopy, time resolved microscopy, reactive multilayers, phase transformations, kinetics, reaction front morphology

Contact Author: Geoffrey H. Campbell, 925-423-8276, ghcampbell@llnl.gov

Total number of pages is 16 and figures is 4

Abstract (250 words)

The Dynamic Transmission Electron Microscope (DTEM) offers a means of capturing rapid evolution in a specimen through in-situ microscopy experiments by allowing 15 ns electron micrograph exposure times. The rapid exposure time is enabled by creating a burst of electrons at the emitter by ultraviolet pulsed laser illumination. This burst arrives a specified time after a second laser initiates the specimen reaction. The timing of the two Q-switched lasers is controlled by high-speed pulse generators with a timing error much less than the pulse duration. Both diffraction and imaging experiments can be performed, just as in a conventional TEM. The brightness of the emitter and the total current control the spatial and temporal resolutions. We have demonstrated 7 nm spatial resolution in single 15 ns pulsed images. These single-pulse imaging experiments have been used to study martensitic transformations, nucleation and crystallization of an amorphous metal, and rapid chemical reactions. Measurements have been performed on these systems that are possible by no other experimental approaches currently available.

Introduction

In-situ microscopy experiments have progressed in recent years in their variety of applications and in the insight they have provided. In some instances it has become obvious that the observations, typically recorded with video methods, lack the time resolution needed to fully interpret the evolution of the specimen. A typical video frame rate is 30 frames per second or 33 ms per frame. A typical goal in the electron microscope during an in-situ experiment is to acquire an image of an evolving microstructure in a specimen that may have moving dislocations or interfaces. For the interpretation of the image, the motion blur of these mobile features must be less than the desired spatial resolution. If it is desired to have the motion blur less than, for example, 10 nm during the 33 ms observation of the video camera, then the speed of the moving feature of interest must be less than 3×10^{-7} m/s ($\sim 1 \times 10^{-6}$ km/h). These speeds are slow when compared to known velocities of important classes of phenomena, such as dislocation speeds during plastic deformation, crystallization fronts in solidification, or interfaces in martensitic and even many diffusional transformations.

Methods to acquire electron microscopic images with much shorter exposure times than video rates have progressed through several stages since the 1960's [1-3], notably from the group of Prof. O. Bostanjoglo at TU Berlin [4]. The methods generally fall into two approaches, stroboscopic and single shot. The stroboscopic method [5-11] has been advanced recently in the lab of Prof. A. Zewail at CalTech [12]. In the recent stroboscopic approach [13, 14], the specimen is

repetitively pumped into a cyclic state by one branch of a femtosecond laser pulsed at a high frequency (MHz or faster) while another branch is used to create a pulse train of electrons that probes the specimen at some particular point in its pump cycle. Each pulse of electrons contains only a small number of electrons (1 to 10^3) and so many pulses are integrated on the detector to build up the image or diffraction pattern. This method has been used to investigate vibrations, bonding, and certain classes of phase transformations[15-17].

In contrast, the single shot imaging method described here, while also following the developments of Bostanjoglo [4, 18-23], acquires an electron micrograph with a single pulse of electrons [24]. The requirement of image formation with a single pulse of electrons places stringent conditions on the electron emission and is controlled, as is usual in electron microscopy, by the brightness of the source [25]. The distinction of single shot imaging is that it can be considered as a "stop action" image, in analogy with photography. This approach can be used on irreversible phenomena in the in-situ experiment. This class of phenomena encompasses many of the areas of interest of the materials scientist. It has been applied to phase transformations [26-29], crystallization [30], and nanowire growth [31]. In principle, this method will be limited in the spatial resolution it can achieve due to space charge and stochastic coulomb interactions between the electrons. However, the current implementation of the technique has not reached this limit. Rather it is source brightness limited, suggesting that further improvements are possible to the spatial resolution over the 7 nm currently demonstrated [32].

Methods

The approach taken with the dynamic transmission electron microscope (DTEM) is to integrate high performance pulsed lasers with the microscope electron optical column [33]. Two pulsed lasers are required, one for electron pulse generation and one for specimen drive. High-speed pulse generators (Stanford DG535®) are used to control the relative timing of the two pulses. Images are acquired on a standard, commercially available charge coupled device (CCD) camera (TVIPS F224HD). Laser alignment, energy, triggering and synchronization with camera acquisition are controlled by motorized optical mounts and a computer-based interface created by custom development within the LabView application package. Operation of the electron microscope is via the usual user interface on the JEOL JEM 2000FX, while one additional custom designed condenser lens is controlled by a voltage controlled power supply.

Electron pulse generation

A custom built, Q-switched, flash lamp pumped Nd:YLF laser is used to create a 25 ns pulse of 1053 nm light with energy as high as 800 mJ that is frequency quintupled to 211 nm and a pulse duration of 12 ns. Free space propagation of the light in air is used between all elements of the optical systems. Computer-controlled, active feedback pointing and centering systems are used to keep the laser on the target at the microscope cathode. The cathode is an 825 μm diameter Ta disk welded to the apex of a Ta wire hairpin on a standard cathode base in the gun of the TEM. This hairpin/disk structure can alternatively be heated to operate the microscope in a conventional thermionic mode. The laser spot size is approximately

350 μm in diameter (full width at half maximum (FWHM)) at the cathode location. The laser is brought to the cathode target through a window placed in the column below the accelerator section. The light enters the column perpendicular to the electron optical axis and is reflected 90° onto the axis by a metal mirror placed inside the column of the microscope. The mirror has a 1 mm hole in its center to allow the electrons to pass through along the electron optical axis. The distance from the final laser focusing lens to the cathode target is 750 mm.

The laser pulse generates on the order of 10^9 electrons at the source, however the source size is of the order 300 μm in diameter. While the brightness is fairly high (estimated at $3x10^7$ $A{\cdot}cm^{-2}{\cdot}steradian^{-1}$), it only operates for approximately 15 ns. Since we require approximately 10^8 electrons falling on the detector to form an image, as many electrons as possible need to be gathered at the cathode and accelerated down the column. Therefore all hard apertures are removed from the accelerator and condenser lens systems, increasing the collection angle. We have also designed and implemented an additional condenser lens to more effectively couple the source through the on-axis mirror and into the column. The end result is a convergent beam of electrons at the specimen that limits the spatial coherence of the illumination and thus becomes the spatial resolution limiting parameter. The steady-state emission current is limited by the Child-Langmuir space charge effect, so that the roughly Gaussian 12 ns FWHM laser pulse produces a roughly flat-topped 15 ns FWHM electron pulse.

For both laser systems, access of the laser light to the vacuum environment of the electron optical column is via laser quality windows on ports. These windows

are made of high purity fused silica and are relatively ineffective at stopping the high energy x-rays generated inside the microscope. Additionally, the extra condenser lens and enhanced electron source coupling substantially increase the current in the column during conventional thermionic emission operations. We have measured steady currents up to 10 μA, compared to microscopes with normal configurations operating with beam currents of order 10 nA. Therefore, substantial lead shielding must be used around the final optics assemblies to block x-rays that escape from the column through these windows.

Specimen reaction initiation

A second laser is used to initiate the reaction of interest in the specimen. It is a Q-switched Nd:YAG laser (Big Sky Lasers, Montana) that emits a 12 ns pulse at 1064 nm with energy to 125mJ. The energy per pulse is controlled by neutral density filters and a motorized half-waveplate and thin film polarizer to tailor the energy for the needs of the experiment. The fundamental wavelength can also be frequency converted to 532 nm or 355 nm, as dictated by the absorption spectrum of the specimen. Again, free space propagation is used and the laser is introduced into the electron optical column through the high angle x-ray analysis port available on the JEOL 2000FX TEM. There is a direct line of sight to the specimen and the final focusing optic is located 600 mm from the specimen. The final spot size of the laser on the specimen depends on the lens focus and the wavelength of light used and is typically 125 μm $1/e^2$ diameter for the fundamental 1064 nm. The spatial profile of the spot on the specimen is essentially Gaussian, however it will be elongated in one direction due to the inclination of 40° from the surface normal plus any additional

tilts put on the specimen holder. This elongation can be partially compensated for by introducing two-fold astigmatism to the laser pulse just before entry into the electron optical column.

Understanding the laser/specimen interaction is key to understanding observations in the DTEM. In most experiments, the laser is used as a localized heat source to rapidly heat the specimen to a certain temperature. The temperature achieved depends on many factors, including the laser pulse energy, specimen reflectance and heat capacity, and specimen thickness. For specimens of constant thickness, the calculation is much more straightforward than for wedge shaped specimens, which may require finite element modeling. Usually, an experimental calibration point is available by the observation of a phase transition, such as melting, at a known temperature [29].

Timing

A computer-controlled master clock controls the timing of all elements of the laser system. The clock controls the relative timing of pulses coming from the two laser systems. The timing jitter in the system is less than 1 ns, which is much shorter than the 12 ns pulse durations for the two lasers. Typically the specimen laser is set to fire first to initiate the response in the specimen and the cathode laser fires at a predetermined time delay later to send the electron pulse through the specimen. This time delay can be set to any time, ranging from 1 ns to 1 ms.

The specimen response as a function of time after the pulsed laser stimulus can be followed in an average sense by performing multiple experiments on fresh areas of the specimen and steadily increasing the time delay. A series of images is then

acquired which, while not tracking the evolution of a particular specimen area, still allows measurements of average quantities. These quantities are then tracked as a function of time after laser irradiation and are useful for comparison to models of materials evolution.

Image recording

A standard commercially available CCD camera is used for recording the single pulse image. The camera has high signal to noise ratio (12:1, defined as signal per primary electron divided by dark noise per pixel) and is single electron sensitive. That is, it is able to detect every incident TEM electron, which is highly advantageous for the signal limited regime of pulsed mode operation. It, too, is controlled through the computer based user interface. When acquiring an image, the camera is typically set to an exposure (integration) time of roughly 1 second, during which the TEM shutter is open, and all of the electrons arrive within a 15 ns period within this 1 s window. Then the camera is read out as in normal operation with the signal originating only from the single pulse of electrons and whatever dark current (thermal, read-out and shot noise) has been accumulated.

Results

Martensitic transformations

Martensitic transformations are modeled as a moving interface that transforms the parent crystal structure into the new crystal structure [34-38]. Details of the interfacial structure have been revealed by *post mortem* investigations of incomplete transformations [39-42]. The DTEM offers the possibility of imaging the moving interface. Ti transforms at elevated temperature from the hexagonal close

packed α crystal structure to the body centered cubic β phase. Figure 1 shows DTEM images of the transformation interface between growing β-phase variants and equi-axed α-phase grains at elevated temperature and again after cooling to room temperature. Further refinement of the β-phase microstructure is observed after cooling due to reverse transformation to the α-phase.

Crystallization reactions

Nickel titanium alloys of nearly equal atomic ratio were sputtered to create amorphous thin film structures for investigation. These films were heated inside the DTEM to temperatures of 1150 K with the specimen treatment laser, which completes the heating within its 12 ns pulse duration. Images were acquired after various delay times as the specimen is crystallizing and an example is shown in Figure 2.

Reactive multilayer foils

Reactive multilayer films (RMLF) are metastable nanostructured combinations of two phases that, upon heating, intermix and react exothermically. The application of a localized source of heat initiates mixing and energy release that creates a self-propagating reaction front that propagates throughout the material, releasing heat to the surroundings. RMLF have found application in material joining and other localized heat source applications [43-48]. One typical system that is used is alternating layers of Al and Ni that when heated will mix and form an intermetallic phase(s) that depends on the overall atomic composition.

To investigate the compositional dependence of the reaction front propagation, we fabricated three multilayer foils varying the relative thickness of the Al and Ni

layers to control the overall composition to 2Ni:3Al, 1Ni:1Al, and 3Ni:2Al atomic ratios. The bilayer period thicknesses were 21 or 25 nm, and 5 or 6 bilayers were deposited to create films of 125 nm in total thickness. The multilayer foils were supported on Cu grids and observed in plan view. The specimen laser was used to heat a localized area of the film and initiate the self-propagating reaction front. Time resolved images at low magnification for all three compositions are shown in Figure 3. The reaction front is clearly discerned in these images, as is the point of origin for the reaction. The distance traveled and the set time delay between initiation and image acquisition are used to calculate the reaction front speed. It was found to be roughly the same for each composition at 13 m/s.

The measured speed of the reaction front can be used to predict its position at a given time relative to the initiation laser pulse. This information is then used to position the field of view in the microscope at high magnification to capture images of the detailed structure of the propagating reaction front. Examples of high magnification images of the reaction fronts are shown in Figure 4.

Discussion

The real space imaging capabilities of the DTEM allow it to generate data that is unavailable through any other time resolved technique. All of the microstructural features in an image that arise from dynamical contrast formation, which are what makes TEM in general such a powerful characterization tool, are also present in the DTEM images. These include dislocations, stacking faults, boundaries and interfaces, as well as the more mundane thickness fringes and bend contours.

These diffraction effects on images are playing the main role in image formation of the crystalline phase within the amorphous matrix of the Ni-Ti thin films. The nucleation events that initiate the crystallization of an amorphous material occur rapidly. The advantage of a real space imaging technique such as DTEM is that it allows the counting of nucleation sites as a function of time after heating the thin foil to quantify average nucleation rates and crystallization kinetics[30]. The image shown in Figure 2 is an example of this type of data that allows for quantitative evaluation of nucleation rates for comparison with models of the process. Reciprocal space (i.e. diffraction) measurements, also possible in the DTEM, give complementary information about phase fractions and crystallography but very little information about morphology.

The image of the interfacial structure of the parent/martensite transformation in Ti reveals a sharply faceted structure (Fig. 1), which is characteristic of this class of shear-distortive phase transformations. This interface morphology is a clear indicator of the nature of the transformation and, again, no other time resolved technique could capture this information.

The morphology of the reactive multilayer foils was also an unexpected result. The exothermic mixing of either the Ni rich or the Al rich systems takes these foils on a trajectory across the phase diagram that intersects a two phase field, inducing phase separation with one of the phases being liquid and the other the B2 intermetallic. The two phases organize themselves into a structure reminiscent of eutectic reaction fronts that may be driven the same capillary forces. Modeling of the reaction had proceeded based on the assumption that the geometry was

essentially planar and two-dimensional [44, 48-51]. This assumption clearly needs to be broadened to include three-dimensional structures.

Conclusions

The DTEM has demonstrated its ability to image the main microstructural features in materials that control their properties and performance. Moreover, it can image these features under dynamic conditions with 15 ns exposure times that enable it to freeze the evolution in time during an in situ experiment. These novel capabilities have allowed new insights into rapid crystallization of amorphous metals, martensitic transformations, and rapid condensed state chemical reactions in energetic multilayer structures.

Acknowledgements

This work performed under the auspices of the Office of Basic Energy Sciences, U.S. Department of Energy by Lawrence Livermore National Laboratory under Contract DE-AC52-07NA27344. We thank Prof. T.P. Weihs for providing the reactive multilayer foils and Prof. D. Grummon for the amorphous NiTi foils.

References

1. King W E, Campbell G H, Frank A, Reed B, Schmerge J F, Siwick B J, Stuart B C and Weber P M 2005. Ultrafast electron microscopy in materials science, biology, and chemistry. *J. Appl. Phys.* **97**, 111101.
2. Spivak G V, Pavlyuchenko O P and Petrov V I 1966. Electron microscopic observation of alterations of the domain structure of magnetic films. *Bull. Acad. Sci., USSR Physical Series* **30**, 822 - 826.
3. Takaoka A and Ura K 1983. Stroboscopic TEM with time resolution of 30 μs. *J. Electron Microsc.* **32**, 299 - 304.
4. Bostanjoglo O 2002. High - speed electron microscopy. *Advances in imaging and electron physics* **121**, 1 - 51.
5. Bostanjoglo O and Rosin T 1976. Stroboscopic study on ultrasonic activity in electron-microscope. *Mikroskopie* **32**, 190-190.
6. Bostanjoglo O and Rosin T 1977. Ultrasonically induced magnetic reversals observed by stroboscopic electron-microscopy. *Optica Acta* **24**, 657-664.
7. Bostanjoglo O and Rosin T 1980. Stroboscopic TEM studies of high-frequency magnetic test materials. *Mikroskopie* **36**, 344-344.
8. Bostanjoglo O and Rosin T 1980. Mass and relaxation-time of domain-walls in thin NiFe films from forced-oscillations. *Journal Of Magnetism And Magnetic Materials* **15-8**, 1529-1530.
9. Bostanjoglo O and Rosin T 1980. Resonance oscillations of magnetic domain-walls and bloch lines observed by stroboscopic electron-microscopy. *Physica Status Solidi A-Applied Research* **57**, 561-568.
10. Bostanjoglo O and Rosin T 1981. Resonance oscillations of bloch lines in permalloy-films. *Physica Status Solidi A-Applied Research* **66**, K5-K10.
11. Bostanjoglo O and Rosin T 1981. New reversal process of neel walls due to nanosecond field pulses. *Physica Status Solidi A-Applied Research* **65**, K117.
12. Zewail a H 2006. 4d ultrafast electron diffraction, crystallography, and microscopy. *Annu. Rev. Phys. Chem.* **57**, 65-103.
13. Lobastov V A, Srinivasan R and Zewail a H 2005. Four - dimensional ultrafast electron microscopy. *Proc. Nat. Acad. Sci.* **102**, 7069 - 7073.
14. Grinolds M S, Lobastov V A, Weissenrieder J and Zewail a H 2006. Four-dimensional ultrafast electron microscopy of phase transitions. *Proc. Nat. Acad. Sci.* **103**, 18427-18431.
15. Barwick B, Park H S, Kwon O H, Baskin J S and Zewail a H 2008. 4d imaging of transient structures and morphologies in ultrafast electron microscopy. *Science* **322**, 1227-1231.
16. Carbone F, Kwon O H and Zewail a H 2009. Dynamics of chemical bonding mapped by energy-resolved 4d electron microscopy. *Science* **325**, 181-184.
17. Flannigan D J, Samartzis P C, Yurtsever A and Zewail a H 2009. Nanomechanical motions of cantilevers: Direct imaging in real space and time with 4d electron microscopy. *Nano Letters* **9**, 875-881.

18. Bostanjoglo O, Elschner R, Mao Z, Nink T and Weingärtner M 2000. Nanosecond electron microscopes. *Ultramicroscopy* **81**, 141 - 147.
19. Dömer H and Bostanjoglo O 2002. Laser ablation of thin films with very high induced stresses. *J. Appl. Phys.* **91**, 5462 - 5467.
20. Dömer H and Bostanjoglo O 2002. Stress effects in laser-pulsed chromium films tracked by nanosecond transmission electron microscopy. *Adv. Eng. Mater.* **4**, 623 - 625.
21. Dömer H and Bostanjoglo O 2003. Phase explosion in laser-pulsed metal films. *Appl. Surf. Sci.* **208 - 209**, 442 - 446.
22. Dömer H and Bostanjoglo O 2003. High-speed transmission electron microscope. *Rev. Sci. Instrum.* **74**, 4369 - 4372.
23. Kleinschmidt H and Bostanjoglo O 2001. Pulsed mirror electron microscope: A fast near-surface imaging probe. *Rev. Sci. Instrum.* **72**, 3898-3901.
24. Lagrange T, Armstrong M R, Boyden K, Brown C G, Campbell G H, Colvin J D, Dehope W J, Frank a M, Gibson D J, Hartemann F V, Kim J S, King W E, Pyke B J, Reed B W, Shirk M D, Shuttlesworth R M, Stuart B C, Torralva B R and Browning N D 2006. Single-shot dynamic transmission electron microscopy. *App. Phys. Lett.* **89**, 044105.
25. Reed B W, Armstrong M R, Browning N D, Campbell G H, Evans J E, Lagrange T and Masiel D J 2008. The evolution of ultrafast electron microscope instrumentation. In: *Annual Meeting on Microscopy and Microanalysis*, pp. 272-281, (Cambridge Univ Press, Albuquerque, NM).
26. Campbell G H, La Grange T B, King W E, Colvin J D, Ziegler A, Browning N D, Kleinschmidt H and Bostanjoglo O 2005. The HCP to BCC phase transformation in Ti characterized by nanosecond electron microscopy. In: *Solid-Solid Phase Transformations in Inorganic Materials*, eds. Howe J M, Lee J K, Laughlin D E, Srolovitz D J and Dahmen U, (TMS, Warrendale,PA, Phoenix, AZ).
27. Kleinschmidt H, Ziegler A, Campbell G H, Colvin J D and Bostanjoglo O 2005. Phase transformation analysis in titanium at nanosecond time resolution. *J. Appl. Phys.*, 054313.
28. Lagrange T, Campbell G H, Colvin J D, Reed B and King W E 2006. Nanosecond time resolved electron diffraction studies of the alpha ->beta in pure Ti thin films using the dynamic transmission electron microscope (DTEM). *J. Mater. Sci.* **41**, 4440-4444.
29. Lagrange T, Campbell G H, Turchi P E A and King W E 2007. Rapid phase transformation kinetics on a nanoscale: Studies of the alpha -> beta transformation in pure, nanocrystalline Ti using the nanosecond dynamic transmission electron microscope. *Acta Mater.* **55**, 5211-5224.
30. Lagrange T, Grummon D S, Reed B W, Browning N D, King W E and Campbell G H 2009. Strongly driven crystallization processes in a metallic glass. *App. Phys. Lett.* **94**, 3.
31. Taheri M L, Lagrange T, Reed B W, Armstrong M R, Campbell G H, Dehope W J, Kim J S, King W E, Masiel D J and Browning N D 2009. Laser-based in situ techniques: Novel methods for generating extreme conditions in TEM samples. *Microsc. Res. Tech.* **72**, 122-130.
32. Lagrange T, Campbell G H, Reed B, Taheri M, Pesavento J B, Kim J S and Browning N D 2007. Nanosecond time-resolved investigations using the in situ of

dynamic transmission electron microscope (DTEM). In: *11th Conference on Frontiers of Electron Microscopy in Materials Science*, pp. 1441-1449, (Elsevier Science Bv, Sonoma, CA).
33. Armstrong M R, Boyden K, Browning N D, Campbell G H, Colvin J D, Dehope W J, Frank a M, Gibson D J, Hartemann F, Kim J S, King W E, Lagrange T B, Pyke B J, Reed B W, Shuttlesworth R M, Stuart B C and Torralva B R 2007. Practical considerations for high spatial and temporal resolution dynamic transmission electron microscopy. *Ultramicroscopy* **107**, 356-367.
34. Bowles J S and Mackenzie J K 1954. The crystallography of martensite transformations .3. Face-centred cubic to body-centred tetragonal transformations. *Acta Metall.* **2**, 224-234.
35. Bowles J S and Mackenzie J K 1954. The crystallography of martensite transformations .1. *Acta Metall.* **2**, 129-137.
36. Hirth J P and Pond R C 1996. Steps, dislocations and disconnections as interface defects relating to structure and phase transformations. *Acta Mater.* **44**, 4749 - 4763.
37. Mackenzie J K and Bowles J S 1954. The crystallography of martensite transformations .2. *Acta Metall.* **2**, 138-147.
38. Pond R C and Hirth J P 1994. Defects at surfaces and interfaces. *Solid State Physics – Advances in Research and Applications* **47**, 287 - 365.
39. Pond R, Jiao H, Zhang L and Aindow M 2006. Accommodation of angular incompatibilities between interfacial facets during precipitate growth. *Metallurgical and Materials Transactions A* **37**, 901.
40. Pond R C, Shang P, Cheng T T and Aindow M 2000. Interfacial dislocation mechanism for diffusional phase transformations exhibiting martensitic crystallography: Formation of TiAl + Ti_3Al lamellae. *Acta Mater.* **48**, 1047.
41. Zhang L and Aindow M 2006. Morphology and interfacial structure of gamma precipitates in the beta phase of a Ti-Al-Nb-Zr alloy. *J. Mater. Sci.* **41**, 611.
42. Zhang L, Zhou T, Aindow M, Alpay S, Blackburn M and Wu M 2005. Nucleation of stress-induced martensites in a Ti/Mo-based alloy. *J. Mater. Sci.* **40**, 2833.
43. Knepper R, Fritz G and Weihs T P 2008. Controlling the shape of Al/Ni multilayer foils using variations in stress. *J. Mater. Res.* **23**, 2009-2016.
44. Knepper R, Snyder M R, Fritz G, Fisher K, Knio O M and Weihs T P 2009. Effect of varying bilayer spacing distribution on reaction heat and velocity in reactive Al/Ni multilayers. *J. Appl. Phys.* **105**, 083504.
45. Nathani H, Wang J and Weihs T P 2007. Long-term stability of nanostructured systems with negative heats of mixing. *J. Appl. Phys.* **101**, 104315.
46. Trenkle J C, Koerner L J, Tate M W, Gruner S M, Weihs T P and Hufnagel T C 2008. Phase transformations during rapid heating of Al/Ni multilayer foils. *App. Phys. Lett.* **93**, 081903.
47. Trenkle J C, Wang J, Weihs T P and Hufnagel T C 2005. Microstructural study of an oscillatory formation reaction in nanostructured reactive multilayer foils. *App. Phys. Lett.* **87**, 153108.
48. Wang J, Besnoin E, Knio O M and Weihs T P 2005. Effects of physical properties of components on reactive nanolayer joining. *J. Appl. Phys.* **97**, 114307.

49. Gunduz I E, Fadenberger K, Kokonou M, Rebholz C and Doumanidis C C 2008. Investigations on the self propagating reactions of nickel and aluminum multilayered foils. *App. Phys. Lett.* **93**, 134101.
50. Gunduz I E, Fadenberger K, Kokonou M, Rebholz C, Doumanidis C C and Ando T 2009. Modeling of the self-propagating reactions of nickel and aluminum multilayered foils. *J. Appl. Phys.* **105**, 074903.
51. Swiston J a J, Besnoin E, Duckham A, Knio O M, Weihs T P and Hufnagel T C 2005. Thermal and microstructural effects of welding metallic glasses by self-propagating reactions in multilayer foils. *Acta Mater.* **53**, 3713.

Figures

Figure 1

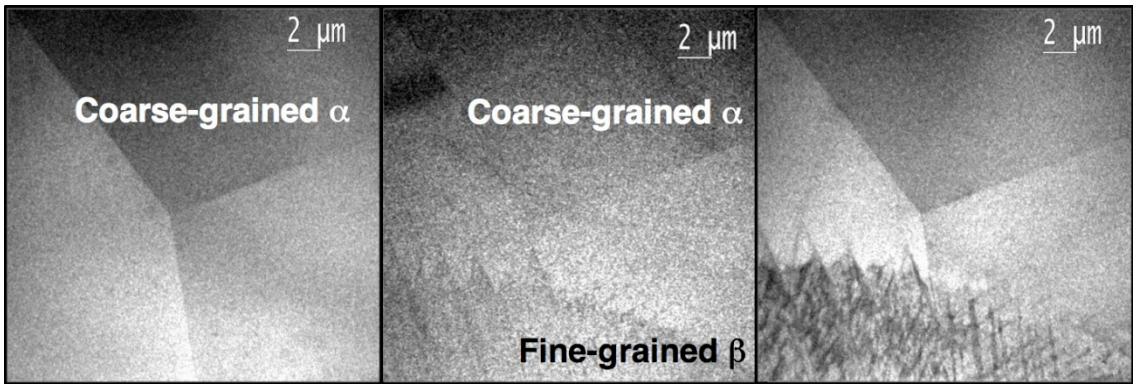

Figure 1 – Time resolved images with 15 ns exposure times of laser irradiated Ti showing the α to β and back to α transformation. The left image (a) shows the course grained initial structure, center (b) shows an image XXnsafter laser irradiation at a spot centered below the area imaged, and at the right (c) shows the specimen after it has cooled again to room temperature and the formerly β region has reverse transformed into fine grained α.

Figure 2

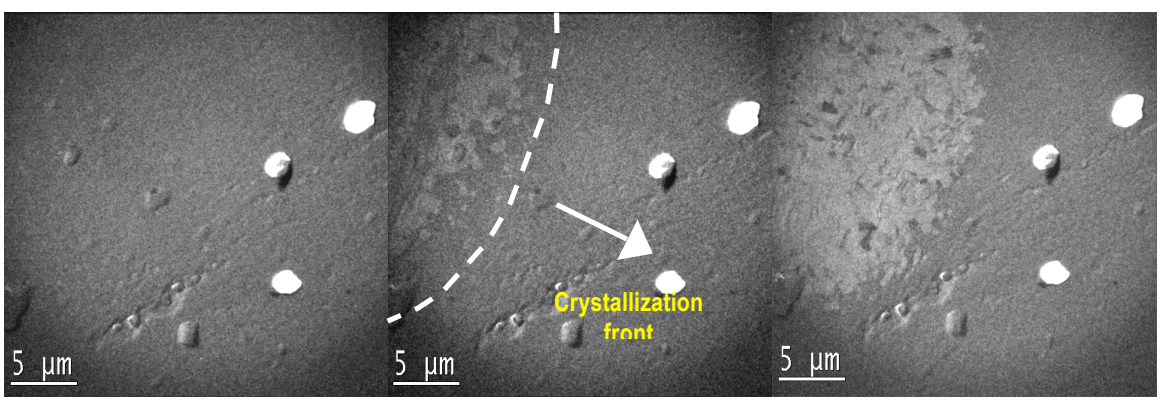

Figure 2 - Time resolved images with 15 ns exposure times of laser irradiated NiTi alloy with initially amorphous structure. Prior to laser irradiation (a) the region of the thin film shows various defects, such as pinholes and surface contours. In (b) the specimen is at elevated temperature (1150K) 1.75 μs after laser irradiation at a spot centered below the imaged area and the crystallized front is seen at the bottom growing into the region. Individual crystal nuclei can be seen forming. In (c) the specimen has crystallized as far as it will go and returned to room temperature.

Figure 3

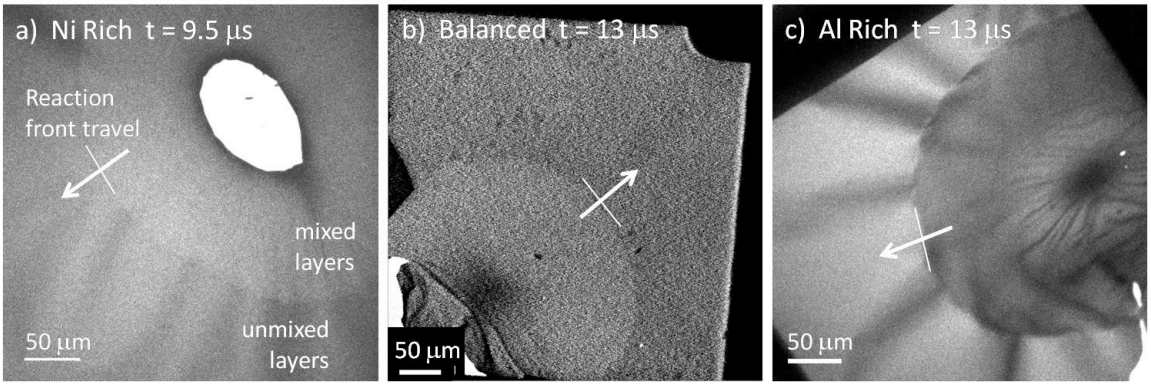

Figure 3 – Low magnification images of reactive multilayer foils, in (a) is the Ni rich composition, (b) the equal atomic ratio composition, and (c) the Al rich composition. The images are acquired at varying times (as indicated) after the 12 ns pulsed laser irradiation clearly capturing the reaction front in the snapshot. The location of the reaction fronts in conjunction with the time delays are used to calculate the reaction front speed.

Figure 4

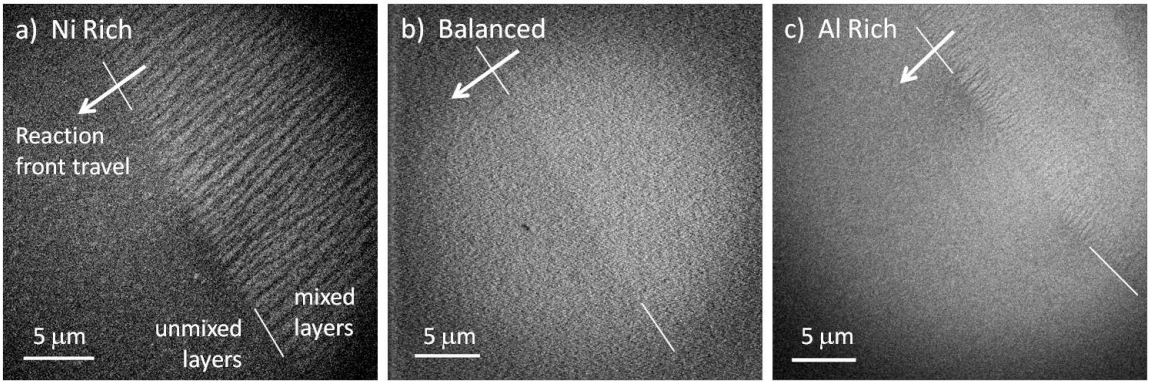

Figure 4 – Time resolved diffraction contrast images with 15 ns exposure times at higher magnification of the propagating reaction front in RMLF specimens. Differences in morphology related to composition are evident in(a) the Ni rich composition, (b) the equal atomic ratio composition, and (c) the Al rich composition (note the fine-scaled phase separation just behind the reaction front). In all three examples, the laser time delays are set to observe the reaction front near the center of view and the electron optic axis.